© 2000 Nature America Inc. • http://structbio.nature.com

The structural basis for red fluorescence in the tetrameric GFP homolog DsRed

Mark A. Wall, Michael Socolich and Rama Ranganathan

Howard Hughes Medical Institute and Department of Pharmacology, The University of Texas Southwestern Medical Center, 5323 Harry Hines Blvd., Dallas, Texas 75390-9050, USA.

Green fluorescent protein (GFP) has rapidly become a standard tool for investigating a variety of cellular activities, and has served as a model system for understanding spectral tuning in chromophoric proteins. Distant homologs of GFP in reef coral and anemone display two new properties of the fluorescent protein family: dramatically red-shifted spectra, and oligomerization to form tetramers. We now report the 1.9 Å crystal structure of DsRed, a red fluorescent protein from *Discosoma* coral. DsRed monomers show similar topology to GFP, but additional chemical modification to the chromophore extends the conjugated π-system and likely accounts for the red-shifted spectra. Oligomerization of DsRed occurs at two chemically distinct protein interfaces to assemble the tetramer. The DsRed structure reveals the chemical basis for the functional properties of red fluorescent proteins and provides the basis for rational engineering of this subfamily of GFP homologs.

Aquatic species such as jellyfish, sea anemones, and coral display an extensive palette of visible fluorescence and coloring. In part, the vibrant coloration is due to a growing family of intrinsically fluorescent proteins[1–3] whose prototypical member is the green fluorescent protein (GFP) from *Aequorea victoria*[4]. GFP is monomeric, soluble, extremely stable, and brightly fluorescent. These properties derive from its tightly packed three-dimensional structure that rigidly holds a chromophore within the core of an eleven-stranded β-barrel[5]. A central feature of GFP is that the chromophore is fully encoded in its amino acid sequence, and is autocatalytically created by a cyclization reaction between residues Ser 65 and Gly 67. Cyclization forms an imidazolin-5-one intermediate that is dehydrogenated at the Cα–Cβ bond of Tyr 66 by molecular oxygen[6] to create the mature chromophore. This chemistry creates a conjugated π-resonance system that largely accounts for the visible absorbance, although energetic interactions between the chromophore and its protein environment help tune the absorbance spectrum. The rigidity and tight packing within the GFP core provide for the high quantum yield of fluorescence by minimizing thermal deactivation of the photoexcited state. Since it is amenable to genetic fusion and modification, GFP is commonly used to study the cellular and tissue distribution of target proteins, to measure intracellular Ca^{2+} concentration or pH at localized sites, and to follow protein folding and protein–protein interactions *in vivo*[7–10].

With regard to spectral tuning of the chromophore by its protein environment, two classes of mechanisms seem to operate in GFP. First, covalent modification of the chromophore through extension of the system of conjugated electrons or through introduction of charge can affect spectral tuning by fundamentally altering the chromophore resonance properties. For example, deprotonation of the phenolic oxygen of the GFP chromophore causes a dramatic red-shifting of chromophore absorbance (nearly 100 nm), and is the mechanism of the fluorescein-like 489 nm absorbance peak of GFP[11,12]. Second, manipulation of electrostatic interactions between the chromophore and its surrounding protein environment mediates spectral tuning by selective interaction with photoexcited or ground states. In the T203Y mutant of GFP, stacking the π-electron system of the tyrosine side chain on the π-electron system of the chromophore[13] causes red-shifting due to relative stabilization of the

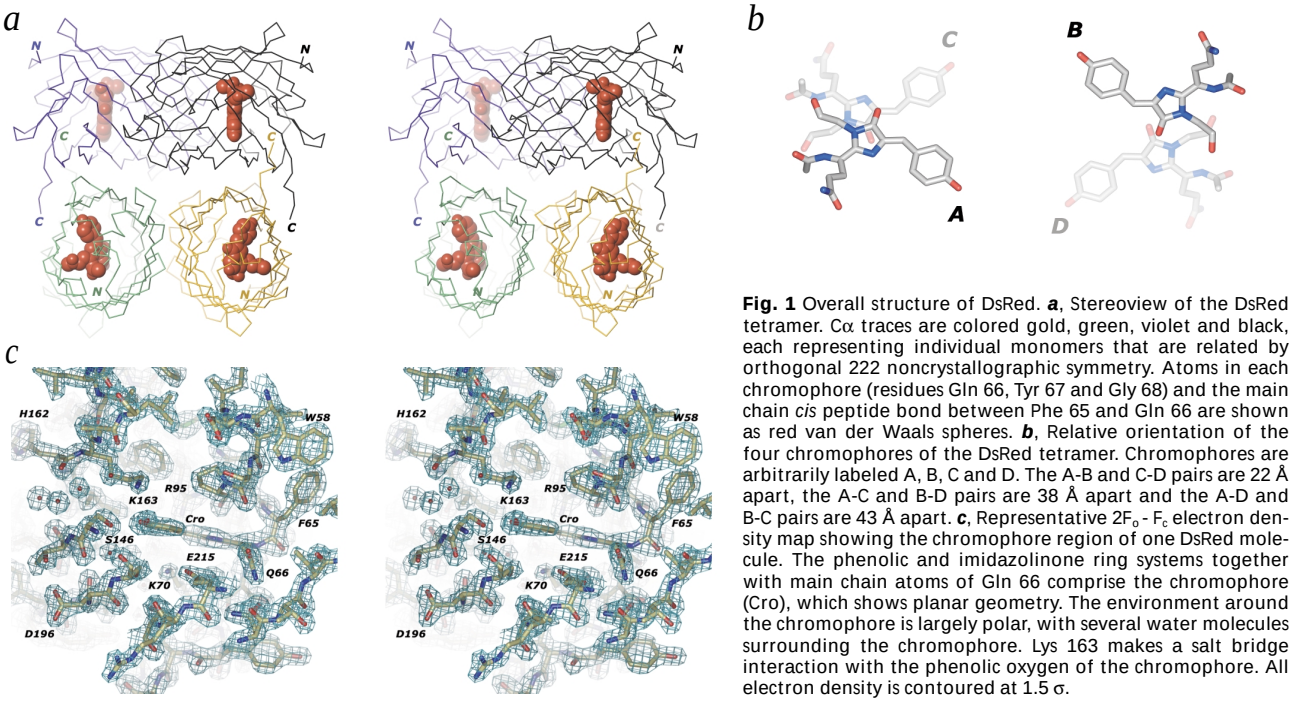

Fig. 1 Overall structure of DsRed. ***a***, Stereoview of the DsRed tetramer. Cα traces are colored gold, green, violet and black, each representing individual monomers that are related by orthogonal 222 noncrystallographic symmetry. Atoms in each chromophore (residues Gln 66, Tyr 67 and Gly 68) and the main chain *cis* peptide bond between Phe 65 and Gln 66 are shown as red van der Waals spheres. ***b***, Relative orientation of the four chromophores of the DsRed tetramer. Chromophores are arbitrarily labeled A, B, C and D. The A-B and C-D pairs are 22 Å apart, the A-C and B-D pairs are 38 Å apart and the A-D and B-C pairs are 43 Å apart. ***c***, Representative $2F_o - F_c$ electron density map showing the chromophore region of one DsRed molecule. The phenolic and imidazolinone ring systems together with main chain atoms of Gln 66 comprise the chromophore (Cro), which shows planar geometry. The environment around the chromophore is largely polar, with several water molecules surrounding the chromophore. Lys 163 makes a salt bridge interaction with the phenolic oxygen of the chromophore. All electron density is contoured at 1.5 σ.

© 2000 Nature America Inc. • http://structbio.nature.com

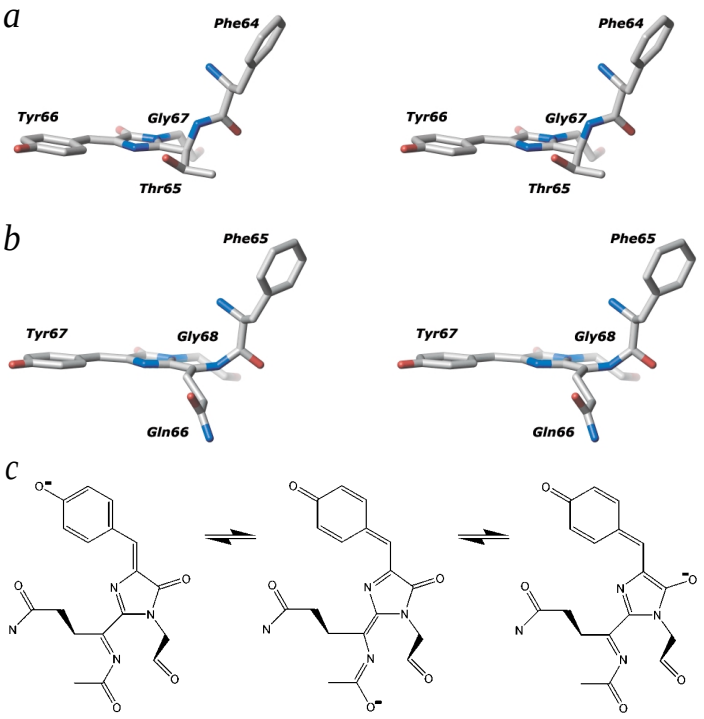

Fig. 2 The chromophore structure of DsRed. Stereoviews of chromophores of ***a***, GFP and ***b***, DsRed,including the immediately N-terminal phenylalanine residue. The perspective is chosen to illustrate the planar architecture of each chromophore and the *trans* (*a*) and *cis* (*b*) peptide bonds preceding the GFP and DsRed chromophores, respectively. ***c***, Proposed resonance species of the DsRed chromophore. Augmentation of the chromophore by dehydrogenation of the Cα-N bond of Gln 66 extends the π-bonding system of electrons to the carbonyl oxygen of Phe 65 through additional resonance structures.

photoexcited state to make yellow fluorescent protein. Similar mechanisms have been shown to mediate spectral tuning in visual opsins and photoactive yellow protein (PYP)[14,15].

While efforts to create GFP mutants differing in emission color have yielded hues of blue (448 nm), cyan (485 nm) and yellow (529 nm), these methods have not yielded longer wavelength absorbing forms[6,16]. However, recently two groups have reported the cloning of several distant GFP homologs in various anthozoa species that include two proteins with highly red-shifted spectra[1–3]. One of these, drFP583, displays a vibrant red fluorescence ($\lambda_{max,absorbance}$= 558 nm, $\lambda_{max,emission}$ = 583 nm) and is commercially available as DsRed (Clontech). Like all of the anthozoa fluorescent proteins, DsRed is a distant homolog of GFP (22% sequence identity). Although likely to have a similar overall topology, the structural basis for the red fluorescence is unknown. However, a recent model for the chromophore in DsRed has been proposed through mass spectrometric analysis of proteolyzed DsRed that suggests extension of the conjugated π-system through an additional dehydrogenation reaction[17]. In addition, this study showed that DsRed is a tetramer in even dilute solutions and it has not been observed to monomerize without protein denaturation.

Here we present the 1.9 Å crystal structure of DsRed and describe the chemical basis for red fluorescence and oligomerization. The chromophore is similar to that in GFP, but is further modified through oxidation of one backbone bond to extend the conjugated π-system. This additional chemistry is accommodated by a rare *cis* configuration that is observed for the peptide bond preceding the chromophore, suggesting peptide bond isomerization as a possible step in chromophore maturation. Oligomerization of DsRed occurs through two protein interfaces that differ dramatically in chemical character. The structure explains the basis for spectral tuning and oligomerization in DsRed and sets the stage for further study and engineering of this new subfamily of GFP-like fluorescent proteins.

Description of the structure

DsRed is an 11-stranded β-can with a central α-helix, nearly identical in topology to the homologous GFP (Fig. 1*a*). Four non-crystallographically related molecules in our $P2_1$ crystals form a tightly packed tetramer with orthogonal 222 symmetry through two extensive protein interaction surfaces. The top and bottom of each β-can is sealed off from bulk solvent by protein atoms, providing a rigid environment within the core of the structure for the DsRed chromophore. The structural rigidity and insulation from bulk solvent are likely key for the efficient quantum yield of fluorescence observed in DsRed[1,19]. As is the case in GFP, the DsRed chromophore rests in the middle of a α-helix that runs through the center of the β-can fold and clearly shares much of the chemical mechanism of formation with GFP, namely autocatalytic cyclization of residues Gln 66, Tyr 67 and Gly 68 and dehydrogenation of the Cα–Cβ bond of Tyr 67 (Figs 1*c*, 2*b*). DsRed monomers comprising one tetramer are highly similar to each other (average root mean square (r.m.s.) deviation of Cα atoms of 0.18 Å), and each monomer differs from *A. victoria* GFP with an average Cα r.m.s. deviation of 1.9 Å. The majority of the backbone structural variation between DsRed and GFP occurs in loop regions that form the ends of the β-can structure.

The oligomeric organization of DsRed suggests the possibility of fluorescence resonance energy transfer (FRET) between chromophores within the tetramers. Indeed, time-resolved anisotropy experiments indicate a rapid phase of depolarization in DsRed that likely results from intratetramer energy transfer[20]. The physical basis for FRET is dipole–dipole coupling between donor and acceptor chromophores, where the probability of energy transfer depends on the spectral overlap between donor emission and acceptor absorbance, and the relative angular displacement and distance between the respective dipoles. Fig. 1*b* shows the relative orientations of chromophores in the DsRed tetramer. The structure shows distances of 22 Å (A–B and C–D) and 38 Å (A–C and B–D) between the indicated chromophore pairs, and 43 Å between the two diagonally related chromophores. If, as in GFP, the chromophore dipole (and transition dipole) lie largely along the bridge between the phenol and imidazolinone rings[21], the angular orientations of these potential FRET pairs in DsRed would be 21°, 47°, and 41°, respectively, suggesting that chromophores A–B and C–D are the most probable FRET pairs. This prediction is in agreement with the fluorescence depolarization measurements in DsRed that suggested relative dipole orientation of ~24° (ref. 20). Nevertheless, precise interpretation of chromophore positions with regard to FRET will require determination of the orientation of transition and ground state dipoles in DsRed relative to the crystallographic model.

DsRed chromophore structure

The chromophore of GFP arises from cyclization of residues Ser 65 and Gly 67 and dehydration to produce the imidazoli-

© 2000 Nature America Inc. • http://structbio.nature.com

© 2000 Nature America Inc. • http://structbio.nature.com

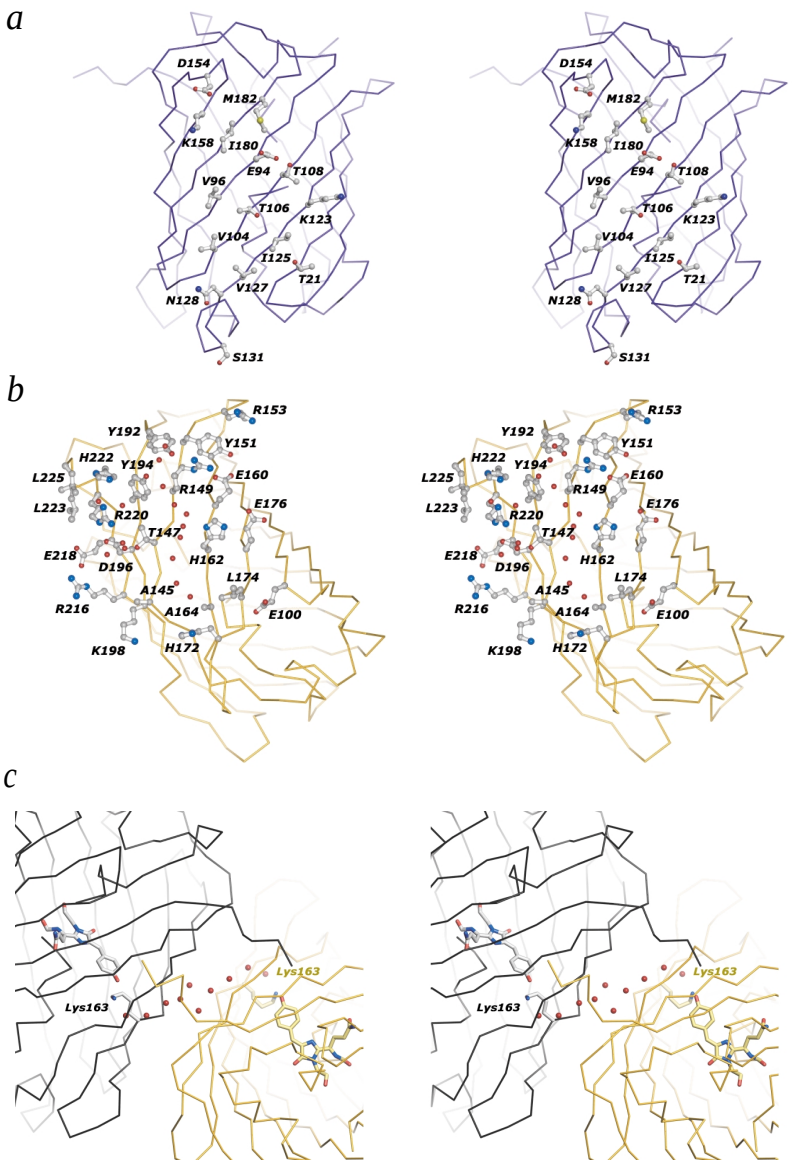

Fig. 3 Stereoview of the DsRed oligomerization interfaces. Two chemically distinct dimerization interfaces occur in the DsRed tetramer. ***a***, One interface contains a central patch of well-packed hydrophobic residues and a largely polar surround, typical for most protein interfaces. ***b***, The other interface is unusually polar, with many ordered water molecules at the center mediating hydrogen-bonding interactions between side chains. The relationship of these interfaces with respect to the tetramer can be seen in Fig. 1*a*; the violet and gold interfaces shown here mediate contact of the similarly colored monomers with the black monomer of Fig. 1*a*. At both interfaces the two-fold rotation axis lies horizontally at the center of the patch of contact residues illustrated, and rotation of the model shown in each figure around that axis will produce the complementary molecule in each dimer pair. ***c***, Stereoview of the solvent path connecting two chromophores across the hydrophilic interface through a hydrogen-bonding network that includes the Lys 163 ε-nitrogen atoms. All waters are fully buried.

none intermediate[6,22,23]. Further dehydrogenation of the Tyr 66 Cα–Cβ bond by molecular oxygen yields a flat chromophore with a π-bonding system that includes two aromatic ring systems and the bridge between them (Fig. 2*a*). A similar mechanism likely operates in DsRed since a *p*-hydroxybenzylideneimidazolinone chromophore system is evident; cyclization of the backbone between Gln 66 and Gly 68 gives rise to the imidazolinone ring which is observed to be planar with the phenolic ring of Tyr 67, indicating dehydrogenation of the Cα–Cβ bond (Fig. 2*b*). However, DsRed shows an additional oxidation reaction at backbone atoms of the Gln 66 residue to extend the conjugated π-electron system. The Gln 66 Cα, originally in sp^3 hybrid (tetrahedral) configuration, is observed to be planar and sp^2 hybridized, consistent with creation of a double bond between Cα and N of position 66 (Fig. 2*b*). The Cα at the identical position in GFP shows normal tetrahedral geometry (Fig. 2*a*)[13,24], indicating that this additional chemistry is specific for DsRed. The extended π-bonding system of the DsRed chromophore yields additional resonance contributors (Fig. 2*c*) resulting in greater delocalization of electrons upon photoexcitation. These structural results are fully consistent with an independent determination of the DsRed chromophore structure through tandem mass spectrometry[17]. Together, these data show that the correctly oriented Gln 66 amide nitrogen and planar Cα augments the π-bonding system in this novel chromophore and suggests that this modification is the structural basis for longer wavelength photon absorbance and emission. A report showing a quantum mechanical calculation of chromophore energetics in DsRed indicates that the extension of the π-electron system accounts quantitatively for its spectral properties[17].

In addition, Phe 65 and Gln 66 of the DsRed chromophore are connected by an unexpected and unique *cis* peptide bond which positions the sp^2 Cα of position 66 in the same plane as the imidazolinone ring and the rest of the chromophore (Figs 1*c*, 2*b*). Modeling of a *trans* peptide bond between these two residues is inconsistent with the crystallographic data and will not permit the additional π-bonded atoms and the chromophore to be coplanar. The analogous positions in GFP show a normal *trans* configuration of this peptide bond (Fig. 2*a*). How does the DsRed protein environment stabilize formation of this unique chromophore structure? *Cis* peptide bonds occur rarely in proteins due to steric repulsion between side chains in the *cis* conformation[25,26]. Rare examples of non-proline *cis* peptide bonds (0.03%) are preceded by β-strand secondary structure and are close to active sites in protein structures[27]. Instances of non-proline *cis* peptide bonds in which the N-terminal residue is aromatic are only found in $(\alpha/\beta)_8$ barrels that show side chain contacts between the two residues sharing the *cis* bond[28–35]. Three factors seem to stabilize the *cis* form of the Phe 65–Gln 66 peptide bond in DsRed: (i) this bond disrupts the middle of the α-helix within the β-can, and due to the secondary structure surrounding the *cis* bond, there is no steric hindrance between the Phe 65 and Gln 66 side chains; (ii) electron delocalization of Gln 66 main chain atoms into the chromophore molecular orbital is a stabilizing influence; and (iii) all potential hydrogen bonds are satisfied upon *trans-cis* isomerization — for example, the carbonyl of Ser 62 (hydrogen-bonded to Gln 66 N in the *trans* state) now forms a hydrogen bond with the ε-nitrogen of

© 2000 Nature America Inc. • http://structbio.nature.com

© 2000 Nature America Inc. • http://structbio.nature.com

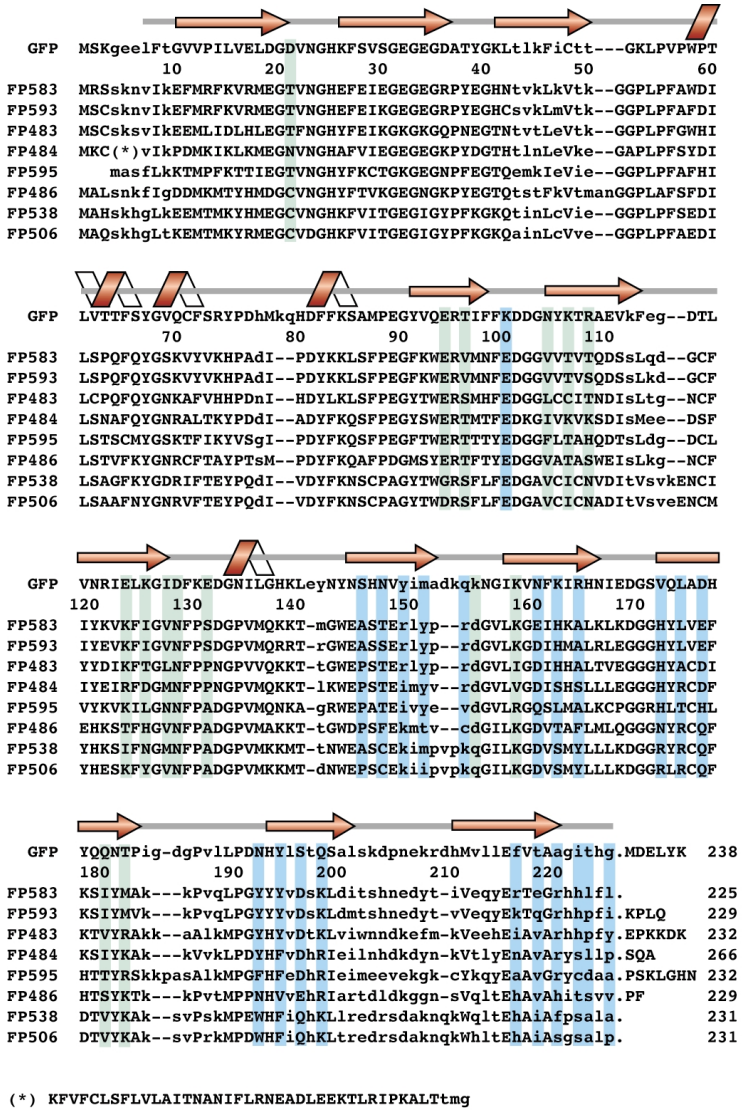

Fig. 4 Structure-based sequence alignment of fluorescent protein family. All homologous sequences (GenBank accession numbers: GFP AAA27721, FP583(DsRed) AF168419, FP593 AF272711, FP483 AF168420, FP484 AF168424, FP595 AF246709, FP486 AF168421, FP538 AF168423 and FP506 AF168422) available in the literature and non-redundant databases are aligned based on superposition of DsRed and GFP structures. Aligned proteins are designated FP### where the three-digit number is the maximum emission wavelength in nanometers. Secondary structure representation of DsRed includes a gray line representing all ordered residues in the DsRed structure. Highlighted residue positions represent side chains lining the hydrophobic dimerization interface (green) and the hydrophilic dimerization interface (blue). Lowercase letters show sequence positions with significant variation, and alignment gaps at individual positions are shown by hyphens (–).

© 2000 Nature America Inc. • http://structbio.nature.com

Gln 213, an interaction that could not occur in GFP since the analogous position contains a leucine.

The observation of a *cis* peptide bond between Phe 65 and Gln 66 in DsRed (but not in GFP) suggests that isomerization around this bond may be a key step in chromophore maturation. Rotation around peptide bonds is energetically disfavored due to their partial double bond character; this is the result of delocalization of the lone-pair electrons of the amide nitrogen in the ground state that creates a polar resonance species with planar geometry. This property results in a ~22 kcal mol^{-1} energy barrier to rotation[36] and restrains the peptide bond to either the *cis* ($\omega = 0^{\circ}$) or *trans* ($\omega = 180^{\circ}$) configuration[37]. Though the energetic interactions described above may stabilize the *cis* configuration of the Phe 65–Gln 66 bond relative to *trans* in DsRed, the rate of achieving this geometry would be expected to be slow given that that bond largely starts in the *trans* state upon folding of the protein. Interestingly, the rate of maturation of red fluorescence in DsRed proceeds with a time course of hours to days[19], consistent with the possibility that peptide bond isomerization may limit the rate of this process. Although all four chromophores in the crystal structure of the DsRed tetramer are seen with identical *cis* peptide bonds between Phe 65 and Gln 66, the equilibrium between *cis* and *trans* may account for a small subpopulation of molecules that continue to exhibit GFP-like absorbance (489 nm) even in the fully mature state[1].

As indicated above, the phenolic oxygen of the wild type GFP chromophore can exist either in the protonated (neutral) or deprotonated (anionic) form, a feature that results in a complex absorbance spectra with two excitation maxima (395 and 489nm). In addition, bulk solvent controls protonation of this site in GFP with an apparent pK_a of 5.8 (ref. 38), indicating some mechanism for proton transfer to the chromophore region. In DsRed, the chromophore is almost certainly strictly anionic since the formally charged ε-nitrogen atom of Lys 163 is observed making a salt bridge interaction with the phenolic oxygen (Fig. 1*c*). Such an interaction would be unlikely to tolerate neutralization of the chromophore even at strongly acidic conditions, consistent with the relative insensitivity of DsRed fluorescence to acidification[19].

Tetramerization interfaces

GFP from *A. victoria* is largely monomeric in aqueous solutions, with a weak propensity for dimerization[24]. In contrast, DsRed is found only as tetrameric and octomeric (much less abundant) species in solution as determined by gel filtration chromatography (not shown), and by analytical ultracentrifugation[19]. Each DsRed molecule contacts the two adjacent monomers on the sides of the β-can, burying 2,268 and 3,210 Å^2 of surface area, respectively. The smaller dimer interface shows characteristics typical of many high-affinity protein–protein interaction surfaces[39]; a set of polar side chains and solvent molecules at the periphery of the interface surround a central cluster of hydrophobic residues that form well-packed van der Waals contacts that fully exclude solvent (Fig. 3*a*). This interface consists of symmetrical residues contributed by one monomer and its copy rotated around a two-fold axis. Given the observed efficiency of atomic packing, these data suggest that this interface may be specifically tuned for homo-oligomeric interaction. The larger interface shows a similar two-fold relationship, including one contact formed by a symmetric extension of C-terminal tails of two monomers as if 'arm-in-arm' (Figs 1*a*, 3*c*). However, this interface is dramatically different in chemical character; 14 buried solvent molecules are found throughout the interface mediating interactions between non-optimally packed residues, and nearly all of the side chains are

© 2000 Nature America Inc. • http://structbio.nature.com

Table 1 DsRed structure determination and refinement

Crystal	Resolution (Å)	Total observed	Unique observed	Completeness (%, highest)	R_{merge}[1] (%, highest)
Native	1.9	525,892	62,456	97.9 (77.0)	8.6 (43.7)
Se-Met	2.3	567,800	70,975	99.9 (99.9)	7.3 (40.1)

SAD phasing (30–2.3 Å)								
Resolution	4.58	3.63	3.18	2.89	2.68	2.52	2.39	2.30
Phasing power[2]	3.05	1.49	0.90	0.62	0.44	0.33	0.26	0.21
Figure of merit	0.49	0.38	0.26	0.17	0.11	0.08	0.06	0.04
After solvent flipping	0.91	0.87	0.82	0.75	0.71	0.74	0.79	0.78

Refinement	30–1.9 Å
Protein atoms	7,132
Solvent atoms	579
R-factor (R_{free})	0.192 (0.212)
Mean B value (Å^2)	18.9
R.m.s deviations from ideal geometry	
Bond lengths (Å)	0.007
Bond angles (°)	1.90
Dihedral angles (°)	26.1
Improper dihedrals (°)	1.01
Ramachandran outliers[3]	0

[1] $R_{merge} = \Sigma|I-\langle I \rangle|/\Sigma I$ where $\langle I \rangle$ is the mean intensity of individual observations.
[2] SAD phasing power is defined as $[<|F^+| - |F^-|>^2/\int_\phi P(\phi)(|F^-|e^{i\phi} + \Delta F| - |F^+|)^2 d\phi]^{1/2}$, where $P(\phi)$ is the experimental phase probability distribution. F^+ and F^- correspond to a Bijvoet pair of structure factors, and ΔF is the difference in heavy atom structure factor.
[3] Residues in generously allowed or disallowed regions. Ramachandran analysis was performed using the program PROCHECK[49].

polar or formally charged (Fig. 3*b*). Such atypical protein interfaces have been observed at oligomerization interfaces that seem to require broader tuning of substrate specificity than that afforded by well-packed van der Waals interactions. For example, the tetramerization domains of eukaryotic K^+ channels display largely polar protein interaction surfaces that mediate the specific hetero-oligomerization of the voltage-gated K^+ channel subunits[40]. Only those subunits within one distinct functional subfamily of K^+ channel subunits oligomerize, a property explained by the conformational plasticity of the polar interactions at the subunit interfaces[41]. An intriguing possibility is that spectrally distinct members of the subfamily of DsRed-like fluorescent proteins may also show hetero-oligomerization *in vivo* as a strategy for producing diversity in coloration and fluorescence emission.

Interestingly, ten of the water molecules sequestered at the polar dimer interface and the ε-nitrogen atoms of symmetrically positioned residues (Lys 163 in two monomers) form a contiguous hydrogen-bonding network isolated from bulk solvent that connects the phenolic oxygens of the two chromophores closest to each other in the tetramer (22 Å apart) (Fig. 3*c*). What is the role of this unusual solvent pathway buried at the protein–protein interface? This network is likely to serve as a stabilizing polar environment to help shield the buried positive charge of Lys 163, the residue forming a salt bridge interaction with the chromophore (Figs 1*c*, 3*c*). This role would be especially important in the photoexcited state, where redistribution of electron density away from the phenolic oxygen[42] would be expected to destabilize Lys 163 by diminishing the favorable electrostatic interaction with the chromophore. Further work through site directed mutagenesis will be required to test the idea that the solvent pathway participates in determining the functional properties of DsRed.

To understand if oligomerization might be a conserved property of members of the coral and anemone GFP-like proteins, we created a structure-based sequence alignment of all available sequences of this family of fluorescent proteins (Fig. 4). Interestingly, this analysis shows that all members of this subfamily share the chemical characteristics of both oligomerization surfaces, and that these surfaces are not well conserved in *A. victoria* GFP. Thus, tetramerization may be a general property of the DsRed-like fluorescent proteins. An interesting possibility is that hetero-oligomerization of DsRed-like proteins may play a role in the diversity of coloration of coral species in the sea through assembly of spectrally distinct subunits.

Conclusions

In this work, we describe the atomic resolution structure of DsRed, a red fluorescing GFP homolog. The structure reveals the chemical basis for red fluorescence and oligomerization in this new subfamily of intrinsically fluorescent proteins and suggests hypotheses for explaining other functional properties of DsRed: slow maturation, stability to changes in external pH, and FRET between subunits. For most biotechnological applications, both the slow maturation and oligomerization of DsRed are undesirable properties that must be addressed through systematic mutagenesis. The availability of the structure and the alignment with the well-characterized GFP should help guide these efforts.

Methods

Protein purification and crystallization. His_6-tagged DsRed (Clontech) was overexpressed using the plasmid $pRSET_B$ in JM109 (DE3) cells in 1 liter of TB broth after being induced with 0.5 mM isopropylthiogalactoside (IPTG) for 18 h at 20 ˚C. Cell paste was resuspended in 60 ml lysis buffer (10 mM imidazole, 0.2 M NaCl, 0.1 M TRIS pH 8.5, 1 mg DNase I and 0.1 mM phenylmethylsulfonyl

© 2000 Nature America Inc. • http://structbio.nature.com

© 2000 Nature America Inc. • http://structbio.nature.com

fluoride (PMSF)), sonicated with a Sonic Dismembrator 550 (Fisher) and centrifuged for 45 min at 18,000 r.p.m. in a Sorvall SS-34 rotor. A total of 2 ml Ni-nitrilotriacetic acid (Ni-NTA) agarose resin (Qiagen) was incubated with the supernatant for 1 h at 4 °C, poured into a column and subsequently washed with 100 ml lysis buffer. Protein was eluted from the Ni-NTA resin with 15 ml elution buffer (200 mM imidazole, 0.2 M NaCl, 10 mM $CaCl_2$ and 0.1 M TRIS pH 8.5), subjected to chymotryptic proteolysis (1:200 mol mol^{-1}) for 18 h at room temperature and reapplied to the Ni-NTA column. DsRed was buffer exchanged into storage buffer (50 mM TRIS pH 8.5, 50 mM LiCl and 2 mM dithiothreitol (DTT)) using an HR10/30 Superdex 75 column (Pharmacia). DsRed was concentrated to 15 mg ml^{-1} using a Centricon 10 (Millipore), flash frozen in liquid nitrogen and stored at -80 ˚C in small aliquots for crystallization trials. Selenomethionyl (SeMet) DsRed was also produced in JM109 (DE3) cells[43] and purified as native DsRed except the storage buffer included 5 mM DTT.

DsRed crystals were obtained after two days at 20 ˚C in hanging drops containing 1 µl of protein and 1 µl of well solution (54% MPD and 0.1 M TRIS pH 8.5). Monoclinic crystals measured 0.06 mm x 0.04 mm x 0.02 mm and belong to the space group $P2_1$ with a = 56.13, b = 129.14, c = 57.45 Å, β = 99.14˚ and four molecules per asymmetric unit. All crystals were flash frozen in liquid propane for data collection.

Structure determination. The crystal structure of DsRed was determined to 2.3 Å using selenomethionine (SeMet) single wavelength anomalous dispersion (SAD) phasing and refined to 1.9 Å with data from a native crystal (Table 1). Data were collected at 100 K with a Molecular Structure Corporation Raxis IV detector (Cu Kα) (native) and with an SBC 3x3 CCD detector at the APS ID19 beamline (SeMet). Diffraction data were indexed and reduced with DENZO[44], and intensities were scaled using SCALEPACK[44]. Automated Patterson search methods implemented in the software Crystallography and NMR System (CNS)[18] were able to identify 20 of the 24 selenium sites in an anomalous Patterson. All further phasing and model refinement steps were also carried out with CNS[18]. The remaining four sites were easily located in an anomalous Fourier map calculated with solvent-flattened phases from the incomplete selenium model. The experimental electron density map, calculated using solvent flattened phases from the complete SAD selenium model, was traceable and clearly showed four molecules per asymmetric unit. Non-crystallographic symmetry (NCS) operators and restraints were never applied during phasing or refinement. All manual model building was performed with O[45]. A randomly selected set of reflections (5%) was flagged for statistical cross-validation purposes (R_{free})[46]. After six rounds of manual rebuilding and subsequent refinement, the model had an R_{free} of 21.2% and an R-value of 19.2% using all observed reflections to 1.9 Å. The chromophore was built after the second refinement round (R_{free} = 0.337) into overlapping $2F_o - F_c$ (contoured to 1.5 σ), $F_o - F_c$ (3.0 σ) and experimental (1.25 σ) electron density. A chromophore was built that included Phe 65 atoms in order to accommodate the unusual *cis* peptide bond leading into an sp^2 hybridized Cα of Gln 66. All computational refinement steps included torsion-angle molecular dynamics[47] followed by positional and temperature factor minimization. The final model contains residues Val 7–Leu 225 (the C-terminus) for all four monomers, and 579 water molecules. The Ramachandran plot shows excellent geometry and no outliers. Buried surface area was calculated using GRASP[48].

Coordinates. The atomic model has been deposited in the Protein Data Bank (accession code 1ggx).

Acknowledgments

We are grateful to Z. Otwinowski for SeMet data collection and initial processing, H. Lee for help preparing crystallization and heavy-atom soak trials, R. Jain, S. Lockless, and M. Machius for insightful discussions, and J. Remington and R. Tsien for communication of data prior to publication. This work was partially supported by a grant from the Robert A. Welch Foundation to R.R., who is also a recipient of the Burroughs-Wellcome Fund New Investigator Award in the Basic Pharmacological Sciences, and is an Assistant Investigator of the Howard Hughes Medical Institute.

Correspondence should be addressed to R.R. *email: rama@chop.swmed.edu*

Received 20 October, 2000; accepted 9 November, 2000.

1. Matz, M.V. *et al. Nature Biotechnol.* **17**, 969–973 (1999).
2. Fradkov, A.F. *et al. FEBS Lett.* **479**, 127–130 (2000).
3. Lukyanov, K.A. *et al. J. Biol. Chem.* **275**, 25879–25882 (2000).
4. Prasher, D.C., Eckenrode, V.K., Ward, W.W., Prendergast, F.G. & Cormier, M.J. *Gene* **111**, 229–233 (1992).
5. Tsien, R.Y. *Annu. Rev. Biochem.* **67**, 509–544 (1998).
6. Heim, R., Prasher, D.C. & Tsien, R.Y. *Proc. Natl. Acad. Sci. USA* **91**, 12501–12504 (1994).
7. Kneen, M., Farinas, J., Li, Y. & Verkman, A.S. *Biophys. J.* **74**, 1591–1599 (1998).
8. Miyawaki, A. *et al. Nature* **388**, 882–7 (1997).
9. Romoser, V.A., Hinkle, P.M. & Persechini, A. *J. Biol. Chem.* **272**, 13270–12374 (1997).
10. Waldo, G.S., Standish, B.M., Berendzen, J. & Terwilliger, T.C. *Nature Biotechnol.* **17**, 691–695 (1999).
11. Heim, R., Cubitt, A.B. & Tsien, R.Y. *Nature* **373**, 663–664 (1995).
12. Chattoraj, M., King, B.A., Bublitz, G.U. & Boxer, S.G. *Proc. Natl. Acad. Sci. USA* **93**, 8362–8367 (1996).
13. Ormö, M. *et al. Science* **273**, 1392–1395 (1996).
14. Kroon, A.R. *et al. J. Biol. Chem.* **271**, 31949–31956 (1996).
15. Kochendoerfer, G.G., Lin, S.W., Sakmar, T.P. & Mathies, R.A. *Trends Biochem. Sci.* **24**, 300–305 (1999).
16. Cubitt, A.B., Woollenweber, L.A. & Heim, R. *Methods Cell Biol.* **58**, 19–30 (1999).
17. Gross, L.A., Baird, G.S., Hoffman, R.C., Baldridge, K.K. & Tsien, R.Y. *Proc. Natl. Acad. Sci. USA* **97**, 11990–11995 (2000).
18. Brunger, A.T. *et al. Acta Crystallogr. D* **54**, 905–921 (1998).
19. Baird, G.S., Zacharias, D.A. & Tsien, R.Y. *Proc. Natl. Acad. Sci. USA* **97**, 11984–11989 (2000).
20. Heikal, A.A., Hess, S.T., Baird, G.S., Tsien, R.Y. & Webb, W.W. *Proc. Natl. Acad. Sci. USA* **97**, 11996–12001 (2000).
21. Bublitz, G., King, B.A. & Boxer, S.G. *J. Am. Chem. Soc.* **120**, 9370–9371 (1998).
22. Cubitt, A.B. *et al. Trends Biochem Sci* **20**, 448–455 (1995).
23. Reid, B.G. & Flynn, G.C. *Biochemistry* **36**, 6786–6791 (1997).
24. Yang, F., Moss, L.G. & Phillips, G.N., Jr. *Nature Biotechnol.* **14**, 1246–1251 (1996).
25. Drakenberg, T. & Forsén, S. *J. Chem. Soc. Chem. Commun.*, 1404–1405 (1971).
26. Radzicka, A., Pedersen, L. & Wolfenden, R. *Biochemistry* **27**, 4538–4541 (1988).
27. Jabs, A., Weiss, M.S. & Hilgenfeld, R. *J. Mol. Biol.* **286**, 291–304 (1999).
28. Dominguez, R. *et al. Nature Struct. Biol.* **2**, 569–576 (1995).
29. Perrakis, A. *et al. Structure* **2**, 1169–1180 (1994).
30. Sakon, J., Adney, W.S., Himmel, M.E., Thomas, S.R. & Karplus, P.A. *Biochemistry* **35**, 10648–10660 (1996).
31. Varghese, J.N. *et al. Proc. Natl. Acad. Sci. USA* **91**, 2785–2789 (1994).
32. Hennig, M. *et al. FEBS Lett* **306**, 80–84 (1992).
33. Wiesmann, C., Beste, G., Hengstenberg, W. & Schulz, G.E. *Structure* **3**, 961–968 (1995).
34. Van Roey, P., Rao, V., Plummer, T.H., Jr. & Tarentino, A.L. *Biochemistry* **33**, 13989–13996 (1994).
35. Terwisscha van Scheltinga, A.C., Hennig, M. & Dijkstra, B.W. *J. Mol. Biol.* **262**, 243–257 (1996).
36. Perricaudet, M. & Pullman, A. *Int. J. Pept. Protein Res.* **5**, 99–107 (1973).
37. Fersht, A.R. *J. Am. Chem. Soc.* **93**, 3504–3515 (1971).
38. Haupts, U., Maiti, S., Schwille, P. & Webb, W.W. *Proc. Natl. Acad. Sci. USA* **95**, 13573–13578 (1998).
39. Clackson, T. & Wells, J.A. *Science* **267**, 383–386 (1995).
40. Kreusch, A., Pfaffinger, P.J., Stevens, C.F. & Choe, S. *Nature* **392**, 945–948 (1998).
41. Bixby, K.A. *et al. Nature Struct, Biol,* **6**, 38–43 (1999).
42. Stewart, R. in *The Proton: Applications to organic chemistry* 228–234 (Academic Press, Orlando, Florida; 1985).
43. Doublie, S. *Methods Enzymol.* **276**, 523–530 (1997).
44. Otwinowski, Z. In *Data collection and processing* (ed. Sawyer, L., Isaacs, N. & Bailey, S.) 56–62 (, SERC Laboratory, Warrington, UK; 1993).
45. Jones, T.A., Zou, J.Y., Cowan, S.W. & Kjeldgaard. *Acta Crystallogr A* **47**, 110–119 (1991).
46. Brunger, A.T. *Nature* **355**, 472–474 (1992).
47. Rice, L.M. & Brunger, A.T. *Proteins* **19**, 277–290 (1994).
48. Nicholls, A., Sharp, K.A. & Honig, B. *Proteins* **11**, 281–296 (1991).
49. Laskowski, R.A., MacArthur, M.W., Moss, D.S. & Thornton, J.M. *J. Appl. Cryst.* **26**, 283–291 (1993).

© 2000 Nature America Inc. • http://structbio.nature.com